

Universal Hydrodynamic Transport Times in the Normal Phase of a Unitary Fermi Gas

Xiang Li, J. Huang, and J. E. Thomas

¹*Department of Physics, North Carolina State University, Raleigh, NC 27695, USA*

(Dated: February 23, 2024)

We determine the hydrodynamic relaxation times τ_η for the shear viscosity and τ_κ for the thermal conductivity in the normal phase of a unitary Fermi gas confined in a box potential. Using a kinetic theory relaxation model, we extract τ_η and τ_κ from the time-dependent free-decay of a spatially periodic density perturbation, yielding the universal density-shift coefficients for the shear viscosity and thermal conductivity.

Measurements of the universal hydrodynamic transport properties of a unitary Fermi gas connect ultracold atoms to nuclear matter [1–3] and provide new challenges to theoretical predictions [4–15]. A unitary Fermi gas is a strongly interacting, scale-invariant, quantum many-body system, created by tuning a trapped, two-component cloud near a collisional (Feshbach) resonance [16]. At resonance, the thermodynamic and transport properties are universal functions of the density and temperature [17], permitting parameter-free comparisons with predictions. Early measurements on expanding Fermi gas clouds with nonuniform density [18, 19] have made way for new measurements in optical box potentials [20], where the density is nearly uniform [21–26]. For a unitary Fermi gas, the second bulk viscosity vanishes, as predicted for scale-invariant systems [27, 28] and demonstrated in experiments on conformal symmetry [29]. Hence, at temperatures above the superfluid transition [30], the normal phase of a unitary gas affords the simplest universal system for hydrodynamic transport measurements, as the static transport properties comprise only the shear viscosity η and the thermal conductivity κ_T .

Remarkably, the measured shear viscosity and thermal conductivity in the normal phase are well fit by the simple expressions [23, 31],

$$\eta = \frac{15}{32\sqrt{\pi}} \frac{(mk_B T)^{3/2}}{\hbar^2} + \alpha_{2\eta} \hbar n_0 \quad (1)$$

and

$$\kappa_T = \frac{15}{4} \frac{k_B}{m} \eta (\alpha_{2\eta} \rightarrow \alpha_{2\kappa}) \quad (2)$$

with k_B the Boltzmann constant and m the atom mass. The density shift coefficients $\alpha_{2\eta}$ and $\alpha_{2\kappa}$ are fit parameters. Here, the temperature T and density n_0 contributions can be understood by dimensional analysis. For the shear viscosity, with a dimension of momentum/area, we expect $\eta \propto \hbar/L^3$, with L a length scale. At high temperature, $L \rightarrow \lambda_T$, the thermal de Broglie wavelength $\propto T^{-1/2}$. At lower temperature, where the cloud is degenerate, $1/L^3 = n_0$. For both η and κ_T , the leading $T^{3/2}$ dependence is obtained by variational calculations for a unitary gas in the two-body Boltzmann limit [4, 6, 12]. Density shifts can be shown to arise from Pauli blocking

in an ideal Fermi gas, but are reduced by in medium effects in a unitary Fermi gas [13]. In contrast to the $T^{3/2}$ coefficients, the density shift coefficients $\alpha_{2\eta}$ and $\alpha_{2\kappa}$ are unknown universal constants in the early stages of measurement, with measured values that are sensitive to the finite hydrodynamic relaxation times.

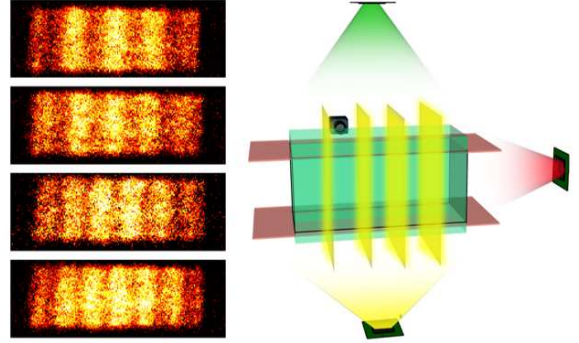


FIG. 1. A unitary Fermi gas is loaded into a repulsive box potential created by two digital micromirror devices DMDs (top, right). A third DMD (bottom) generates a static spatially periodic perturbation δU with an adjustable wavelength, creating spatially periodic 1D density profiles (left). After δU is abruptly extinguished, the dominant Fourier component exhibits an oscillatory decay (see Fig. 2).

In this work, we employ a hydrodynamic relaxation model based on kinetic theory to extract of the universal hydrodynamic relaxation times τ_η and τ_κ from the measured time-dependent free-decay of a spatially periodic density perturbation in a unitary Fermi gas. The extracted relaxation times determine the static shear viscosity and thermal conductivity, yielding the two universal density shift parameters $\alpha_{2\eta}$, $\alpha_{2\kappa}$, corrected for the finite response time over which the viscous force and heat current relax to their Navier-Stokes forms.

The experiments employ ultracold ^6Li atoms in a balanced mixture of the two lowest hyperfine states, which are evaporatively cooled in a CO_2 laser trap and loaded into a box potential, Fig. 1, producing a sample of nearly uniform density n_0 . The box comprises six sheets of blue-detuned light, created by two digital micromirror devices (DMDs) [21, 23] (top and right). The box potential $U_0(\mathbf{r})$ yields a rectangular density profile with typical dimen-

sions $(x, y, z) = (52 \times 50 \times 150) \mu\text{m}$. The density varies slowly in the direction of the long (z) axis, due to the harmonic confining potential $\propto z^2$ arising from the curvature of the bias magnetic field, which has little effect on the shorter x and y axes. The typical total central density is $n_0 = 3.3 \times 10^{11}$ atoms/cm³, with the Fermi energy $\epsilon_F \equiv k_B T_F = k_B \times 0.18 \mu\text{K}$ and Fermi speed $v_F \simeq 2.25$ cm/s. The box depth $U_0 \simeq 0.75 \mu\text{K}$ (see Ref. [23]).

We add a third DMD Fig. 1 (bottom) to independently project a static optical potential δU that spatially varies with an adjustable wavelength λ along one axis, creating a sinusoidal density perturbation. Once equilibrium is established, the perturbing potential is abruptly extinguished, causing an oscillatory decay of the measured density perturbation $\delta n(z, t) = n(z, t) - n_0(z)$. By performing a fast Fourier transform (FFT) of $\delta n(z, t)$ at each time, in a region containing an integer number (typically 3-4) of spatial periods, we obtain $\delta n(q, t)$, Fig. 2.

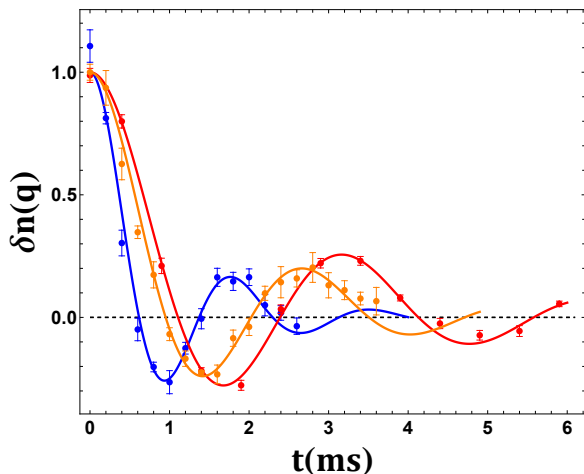


FIG. 2. Fourier component of the density perturbation $\delta n(q, t)$ with $q = 2\pi/\lambda$, for wavelengths $\lambda = 40.0 \mu\text{m}$, $31.3 \mu\text{m}$, and $22.7 \mu\text{m}$, at reduced temperatures $T/T_F = 0.42, 0.36$, and 0.32 , respectively. Dots (data); Curves: hydrodynamic relaxation time model. The error bars are the standard deviation of the mean of $\delta n(q, t)$ for 5-8 runs, taken in random time order.

As shown previously [23], $\delta n(q, t)$ contains a thermally diffusive mode ($\simeq 30\%$) that decays at a rate $\propto \kappa_T$ and an oscillating first sound mode, which decays at a rate dependent on both η and κ_T . The relaxation model determines the response of the viscous force and heat current at the first sound frequency in the sound mode, as well as the response of the heat current at the decay rate in the thermally diffusive mode.

We derive the relaxation model in the linear response regime by constructing four coupled equations: two describe the changes in the density $\delta n(z, t)$ and temperature $\delta T(z, t)$, and two describe the relaxation of the viscous force and heat current. We ignore the box potential, since we measure the free-decay over time scales that avoid perturbing $\delta n(z, t)$ in the measured central region by reflections from the boundaries. After the perturbing

potential is extinguished, the density change obeys [31],

$$\delta \ddot{n} = c_T^2 \partial_z^2 (\delta n + \delta \tilde{T}) + \delta Q_\eta. \quad (3)$$

The first term in Eq. 3 arises from the pressure change with c_T the isothermal sound speed, and

$$\delta \dot{Q}_\eta + \frac{1}{\tau_\eta} \delta Q_\eta = \frac{4}{3} \frac{p}{mn_0} \partial_z^2 \delta \dot{n} \quad (4)$$

describes the relaxation of the viscous damping force [31]. Here the pressure is $p = \frac{2}{5} n \epsilon_F f_E(\theta)$, where the universal function $f_E(\theta)$ has been measured [30], n_0 is the background density, and we have used the continuity equation to eliminate the velocity field. For fast relaxation, Eq. 4 yields the usual Navier-Stokes form for δQ_η in Eq. 3 with $\eta = \tau_\eta p$ the static shear viscosity, independent of the single particle phase space distribution [31].

In Eq. 3, we have defined a scaled temperature, $\delta \tilde{T} = n_0 \beta \delta T$ with a dimension of density, where $\beta = -1/n(\partial n/\partial T)_P$ is the thermal expansivity [31]. We find

$$\delta \dot{\tilde{T}} = \epsilon_{LP} \delta \dot{n} + \delta Q_\kappa. \quad (5)$$

The first term describes the adiabatic change in the temperature with $\epsilon_{LP} \equiv c_{P1}/c_{V1} - 1$ the Landau-Placzek parameter. The heat capacities per particle at constant volume c_{V1} and at constant pressure c_{P1} are determined by the measured equation of state $f_E(\theta)$ [30, 31] and

$$\delta \dot{Q}_\kappa + \frac{1}{\tau_\kappa} \delta Q_\kappa = \frac{5}{2} \frac{k_B}{m} \frac{p}{n_0 c_{V1}} \partial_z^2 \delta \tilde{T} \quad (6)$$

describes the relaxation of the heat current. For fast relaxation, Eq. 6 yields the usual heating rate δQ_κ in Eq. 5 with $\kappa_T = \frac{5}{2} \frac{k_B}{m} \tau_\kappa p$ the static thermal conductivity. Here, the factor $5/2$ is dependent on a Maxwell-Boltzmann approximation for the single particle phase space distribution [31].

A spatial Fourier transform of Eqs. 3-6 yields coupled linear equations for $\delta \ddot{n}(q, t)$, $\delta \dot{\tilde{T}}(q, t)$, $\delta \dot{Q}_\eta(q, t)$, and $\delta \dot{Q}_\kappa(q, t)$ with $q = 2\pi/\lambda$. As the system is initially in mechanical equilibrium and isothermal, only $\delta n(q, 0) \equiv A \neq 0$. Fig. 2 shows fits of the relaxation model (solid curves) to typical data (scaled by $1/A$), where the fit parameters are $c_T q$, τ_η , τ_κ , and the amplitude A . As in our previous work [23], the wavelength of the perturbation and the fit frequency $c_T q$ self-consistently determine the sound speed c_T and the corresponding reduced temperature $T/T_F = \theta(c_T/v_F)$ from $f_E(\theta)$, with the Fermi speed v_F given for the average central density n_0 [31].

Our extracted relaxation times τ_η for the shear viscosity and τ_κ for the thermal conductivity are shown as functions of $\theta = T/T_F$ in Fig. 3. The relaxation times are given in units of the Fermi time $\tau_F \equiv \lambda_F/v_F = \pi \hbar/\epsilon_F \simeq 120 \mu\text{s}$. The wavelength dependence of τ_η and τ_κ is shown for $\theta \simeq 0.30$, demonstrating negligible λ -dependence as expected. As discussed below, the fitted density shift coefficients $\alpha_\eta > \alpha_\kappa$ make $\tau_\kappa/\tau_\eta \simeq 1.2$ for $\theta \simeq 0.4$, deviating significantly from the high temperature limit (dashed red curves), where $\tau_\kappa/\tau_\eta = 3/2$ [13, 31].

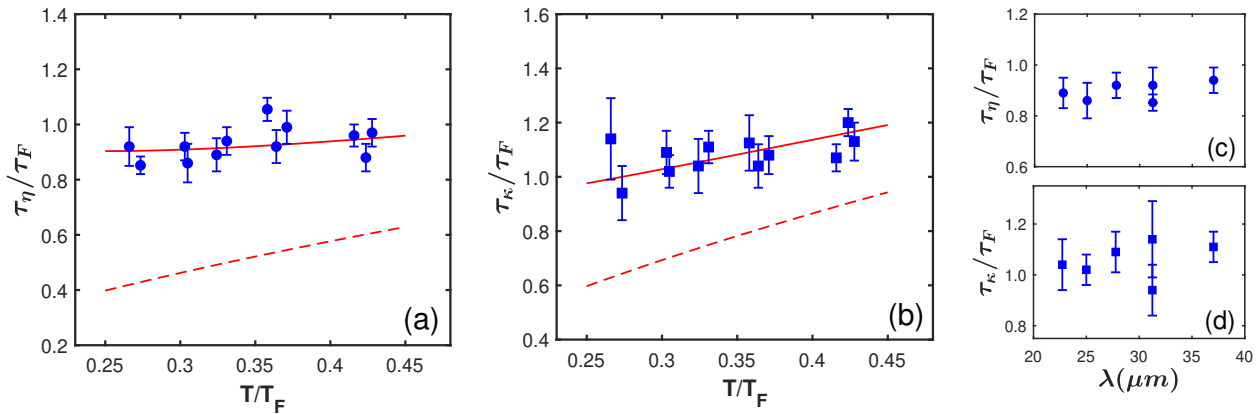


FIG. 3. Hydrodynamic relaxation times in units of the Fermi time $\tau_F \equiv \lambda_F/v_F = \pi\hbar/\epsilon_F$ versus reduced temperature T/T_F . a) τ_η for the shear viscosity (blue circles). b) τ_κ for the thermal conductivity (blue squares). Red curves include the density shift coefficients $\alpha_{2\eta} = 0.45$ and $\alpha_{2\kappa} = 0.22$. Red dashed curves: High temperature limits, where $\alpha_{2\eta} = 0$ and $\alpha_{2\kappa} = 0$ and $\tau_\kappa/\tau_\eta = 3/2$. (c,d) Wavelength dependence for $\theta \simeq 0.30$. Error bars are statistical [32]. (color online)

The measured τ_η determines the static shear viscosity $\eta = \tau_\eta p$ shown in Fig. 4 a (Blue circles). Eq. 1, in units of $\hbar n_0$, gives

$$\eta(\theta) = \alpha_{3/2} \theta^{3/2} + \alpha_{2\eta}, \quad (7)$$

where $\alpha_{3/2} = \frac{45\pi^{3/2}}{64\sqrt{2}} \simeq 2.77$ [4, 6, 12]. The red curve in Fig. 4 a shows the fit for $\eta(\theta)$ with the density shift coefficient $\alpha_{2\eta}$ as the only fit parameter, yielding $\alpha_{2\eta} = 0.45(04)$. Fig. 3 a shows the corresponding curve for $\tau_\eta = \eta/p$, with $p = \frac{2}{5}n\epsilon_F f_E(\theta)$. The red-dashed curve in Fig. 4 a is the high temperature limit, $\alpha_{2\eta} = 0$.

Similarly, the measured τ_κ determines the static thermal conductivity $\kappa_T = \frac{5}{2} \frac{k_B}{m} \tau_\kappa p$ shown in Fig. 4 b (Blue squares). In the high temperature two-body Boltzmann limit, one can show that $\tau_\kappa/\tau_\eta = 3/2$ for any isotropic collision cross section $d\sigma/d\Omega$, so that $\kappa_T = \frac{15}{4} \frac{k_B}{m} \eta$. Eq. 2, in units of $n_0 \hbar k_B/m$, gives

$$\kappa_T(\theta) = \frac{15}{4} (2.77 \theta^{3/2} + \alpha_{2\kappa}). \quad (8)$$

The red curve in Fig. 4 b shows the fit of $\kappa_T(\theta)$ with the density shift coefficient $\alpha_{2\kappa}$ as the only fit parameter, yielding $\alpha_{2\kappa} = 0.22(03)$, i.e., the shift is $15/4 \times 0.22$ in units of $n_0 \hbar k_B/m$. Fig. 3 b shows the corresponding curve for $\tau_\kappa = \frac{2}{5} \frac{m}{k_B} \kappa_T/p$. The red-dashed curve in Fig. 4 b is the high temperature limit, $\alpha_{2\kappa} = 0$.

Finally, Fig. 4 c shows the corresponding first sound diffusivity [31, 33] D_1 in units of \hbar/m . The measured transport times determine $D_1 = \frac{8}{15} \tau_\eta \frac{\epsilon_F}{\hbar} f_E(\theta) + \frac{2}{3} \tau_\kappa \frac{\epsilon_F}{\hbar} \theta$ (Blue triangles). The red-solid curve gives D_1 in terms of the fits for the static shear viscosity and thermal conductivity $D_1 = 4/3 (2.77 \theta^{3/2} + 0.45) + (n k_B T/p) (2.77 \theta^{3/2} + 0.22)$. Here, the thermal conductivity contribution includes a factor $(n k_B T/p)$ for the unitary gas, where p

is the pressure [31]. The red-dashed curve is the high temperature limit $D_1 = 7/3 \times 2.77 \theta^{3/2}$.

In conclusion, we have used a kinetic theory model to extract the transport relaxation times for the shear viscosity and thermal conductivity of a normal-phase unitary Fermi gas in a box potential. The relaxation times of the thermal current and viscous force are found to be comparable to the Fermi time λ_F/v_F , small, but not negligible, compared to the time scales for the oscillatory decay of the density perturbation. The measured transport times enable new estimates of the universal density shift corrections for both the static shear viscosity, $\Delta\eta = n_0 \hbar \alpha_{2\eta}$ with $\alpha_{2\eta} = 0.45(04)$ and the static thermal conductivity $\Delta\kappa_T = n_0 \hbar \frac{k_B}{m} \frac{15}{4} \alpha_{2\kappa}$, where $\alpha_{2\kappa} = 0.22(03)$. For the measured range of θ , our τ_η and η are in reasonable agreement with the predictions of Enss et al., see Figs. 6 (where $\tau_F \equiv \hbar/\epsilon_F$) and 7 of Ref. [8]. However, the measured values of κ_T are significantly smaller than predicted in [13] and larger than predicted in [15]. It can be shown that density shifts of η and κ_T , i.e., $\alpha_{2\eta}$ and $\alpha_{2\kappa}$, arise from Pauli blocking in an ideal Fermi gas. However, the results for the ideal gas are too large and are mitigated by strong interactions in a unitary Fermi gas [13]. Our measurements emphasize the need for improved calculations of the leading density-dependent corrections to the hydrodynamic transport properties as well as more sophisticated relaxation models.

We thank Thomas Schäfer for stimulating discussions and Ilya Arakelyan for help with the new optical system. Primary support for this research is provided by the National Science Foundation (PHY-2006234 and PHY-2307107). Additional support is provided by the Air Force Office of Scientific Research (FA9550-22-1-0329).

*Corresponding author: jethoma7@ncsu.edu

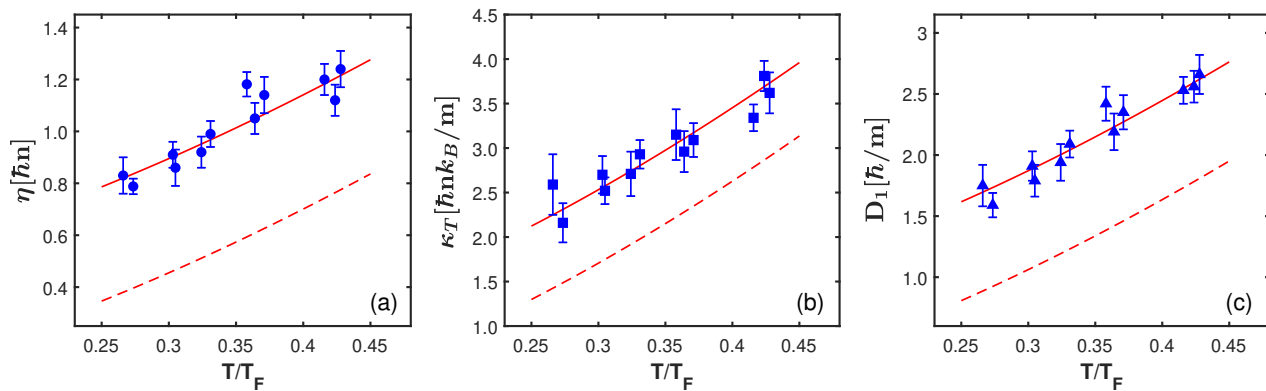


FIG. 4. Transport properties obtained from the measured transport times τ_η and τ_κ versus reduced temperature $\theta = T/T_F$. a) Shear viscosity (Blue circles). b) Thermal conductivity (Blue squares). c) First sound diffusivity (Blue Triangles). Red solid curves include the density shift coefficients $\alpha_{2\eta} = 0.45$ in Eq. 7 and $\alpha_{2\kappa} = 0.22$ in Eq. 8. Red-dashed curves are the high temperature limits, where $\alpha_{2\eta} = 0$ and $\alpha_{2\kappa} = 0$. Error bars are statistical. (color online)

-
- [1] A. Adams, L. D. Carr, T. Schäfer, P. Steinberg, and J. E. Thomas, Strongly correlated quantum fluids: ultracold quantum gases, quantum chromodynamic plasmas and holographic duality, *New J. Phys.* **14**, 115009 (2012).
- [2] I. Bloch, J. Dalibard, and S. Nascimbène, Quantum simulations with ultracold quantum gases, *Nature Physics* **8**, 267 (2012).
- [3] G. C. Strinati, P. Pieri, G. Röpke, P. Schuck, and M. Urban, The BCS-BEC crossover: From ultra-cold Fermi gases to nuclear systems, *Physics Reports* **738**, 1 (2018).
- [4] G. M. Bruun and H. Smith, Shear viscosity and damping for a Fermi gas in the unitary limit, *Phys. Rev. A* **75**, 043612 (2007).
- [5] E. Taylor and M. Randeria, Viscosity of strongly interacting quantum fluids: Spectral functions and sum rules, *Phys. Rev. A* **81**, 053610 (2010).
- [6] M. Braby, J. Chao, and T. Schäfer, Thermal conductivity and sound attenuation in dilute atomic Fermi gases, *Phys. Rev. A* **82**, 033619 (2010).
- [7] M. Braby, J. Chao, and T. Schäfer, Viscosity spectral functions of the dilute fermi gas in kinetic theory, *New Journal of Physics* **13**, 035014 (2011).
- [8] T. Enss, R. Haussmann, and W. Zwerger, Viscosity and scale invariance in the unitary Fermi gas, *Annals Phys.* **326**, 770 (2011).
- [9] H. Guo, D. Wulin, C.-C. Chien, and K. Levin, Microscopic approach to shear viscosities of unitary Fermi gases above and below the superfluid transition, *Phys. Rev. Lett.* **107**, 020403 (2011).
- [10] G. Wlazłowski, P. Magierski, and J. E. Drut, Shear viscosity of a unitary Fermi gas, *Phys. Rev. Lett.* **109**, 020406 (2012).
- [11] P. Romatschke and R. E. Young, Implications of hydrodynamic fluctuations for the minimum shear viscosity of the dilute Fermi gas at unitarity, *Phys. Rev. A* **87**, 053606 (2013).
- [12] M. Bluhm, J. Hou, and T. Schäfer, Determination of the density and temperature dependence of the shear viscosity of a unitary Fermi gas based on hydrodynamic flow, *Phys. Rev. Lett.* **119**, 065302 (2017).
- [13] B. Frank, W. Zwerger, and T. Enss, Quantum critical thermal transport in the unitary Fermi gas, *Phys. Rev. Research* **2**, 023301 (2020).
- [14] J. Hofmann, High-temperature expansion of the viscosity in interacting quantum gases, *Phys. Rev. A* **101**, 013620 (2020).
- [15] H. Zhou and Y. Ma, Thermal conductivity of an ultracold Fermi gas in the BCS-BEC crossover, *Sci. Rep.* **11**, 1228 (2021).
- [16] K. M. O'Hara, S. L. Hemmer, M. E. Gehm, S. R. Granade, and J. E. Thomas, Observation of a strongly interacting degenerate Fermi gas of atoms, *Science* **298**, 2179 (2002).
- [17] T.-L. Ho, Universal thermodynamics of degenerate quantum gases in the unitarity limit, *Phys. Rev. Lett.* **92**, 090402 (2004).
- [18] C. Cao, E. Elliott, J. Joseph, H. Wu, J. Petricka, T. Schäfer, and J. E. Thomas, Universal quantum viscosity in a unitary Fermi gas, *Science* **331**, 58 (2011).
- [19] J. A. Joseph, E. Elliott, and J. E. Thomas, Shear viscosity of a unitary Fermi gas near the superfluid phase transition, *Phys. Rev. Lett.* **115**, 020401 (2015).
- [20] N. Navon, R. P. Smith, and Z. Hadzibabic, Quantum gases in optical boxes, *Nat. Phys.* **17**, 1334 (2021).
- [21] L. Baird, X. Wang, S. Roof, and J. E. Thomas, Measuring the hydrodynamic linear response of a unitary Fermi gas, *Phys. Rev. Lett.* **123**, 160402 (2019).
- [22] P. B. Patel, Z. Yan, B. Mukherjee, R. J. Fletcher, J. Struck, and M. W. Zwierlein, Universal sound diffusion in a strongly interacting Fermi gas, *Science* **370**, 1222 (2020).
- [23] X. Wang, X. Li, I. Arakelyan, and J. E. Thomas, Hydrodynamic relaxation in a strongly interacting Fermi gas, *Phys. Rev. Lett.* **128**, 090402 (2022).
- [24] X. Li, X. Luo, S. Wang, K. Xie, X.-P. Liu, H. Hu, Y.-A. Chen, X.-C. Yao, and J.-W. Pan, Second sound attenuation near quantum criticality, *Science* **375**, 528 (2022).
- [25] H. Hu, P. Zou, and X.-J. Liu, Low-momentum dynamic

- structure factor of a strongly interacting Fermi gas at finite temperature: A two-fluid hydrodynamic description, *Phys. Rev. A* **97**, 023615 (2018).
- [26] Z. Yan, P. B. Patel, B. Mukherjee, C. J. Vale, R. J. Fletcher, and M. W. Zwierlein, Thermography of the superfluid transition in a strongly interacting Fermi gas, *Science* **383**, 629 (2024).
- [27] D. T. Son, Vanishing bulk viscosities and conformal invariance of the unitary Fermi gas, *Phys. Rev. Lett.* **98**, 020604 (2007).
- [28] Y.-H. Hou, L. P. Pitaevskii, and S. Stringari, Scaling solutions of the two-fluid hydrodynamic equations in a harmonically trapped gas at unitarity, *Phys. Rev. A* **87**, 033620 (2013).
- [29] E. Elliott, J. A. Joseph, and J. E. Thomas, Observation of conformal symmetry breaking and scale invariance in expanding Fermi gases, *Phys. Rev. Lett.* **112**, 040405 (2014).
- [30] M. Ku, A. T. Sommer, L. W. Cheuk, and M. W. Zwierlein, Revealing the superfluid lambda transition in the universal thermodynamics of a unitary Fermi gas, *Science* **335**, 563 (2012).
- [31] See the Supplemental Material for discussion of the linearized hydrodynamic equations, the kinetic theory relaxation model, and the determination of the static transport properties.
- [32] The vertical error bars in Figs. 3 and 4 denote $\pm\sqrt{2\epsilon_{ii}}$, where ϵ_{ij} is the error matrix obtained from $\chi^2(\tau_\eta, \tau_\kappa)$ with A and c_T fixed.
- [33] L. D. Landau and E. M. Lifshitz, *Fluid Dynamics, Course of Theoretical Physics Vol. VI* (Pergamon Press, Oxford, 1959).

Appendix A: Supplemental Material

In this supplemental material, we derive a kinetic theory relaxation model, which is used to extract the hydrodynamic transport times τ_η for the shear viscosity and τ_κ for the thermal conductivity from the measured free oscillatory decay of a spatially periodic density perturbation in a normal fluid unitary Fermi gas.

1. Hydrodynamic linear response for a normal fluid.

We consider a normal phase unitary Fermi gas, which is a single component fluid with a mass density $\rho \equiv nm$, where n is the total particle density (we assume a 50-50 mixture of two components) and m is the atom mass. $\rho(\mathbf{r}, t)$ satisfies the continuity equation,

$$\partial_t \rho + \partial_i(\rho v_i) = 0, \quad (\text{S1})$$

where a sum over $i = x, y, z$ is implied. The mass flux (momentum density) is ρv_i , with $v_i(\mathbf{r}, t)$ the velocity field.

Our experiments measure the response of the density in the central region of the box over short enough time scales that forces arising from the walls of the box potential can be neglected. As the perturbing potential $\delta U = 0$ during the measured evolution, the momentum density and corresponding momentum flux $\rho v_i v_j$ obey

$$\partial_t(\rho v_i) + \partial_j(\rho v_i v_j) = -\partial_i p - \partial_j p_{ij}^1, \quad (\text{S2})$$

where $-\partial_i p$ is the force per unit volume arising from the scalar pressure p and $\partial_j p_{ij}^1$ is the viscous force per unit volume, which we determine using a kinetic theory relaxation model in S A 2. Taking the divergence of eq. S2, and using eq. S1, we immediately obtain

$$-\partial_t^2 \rho + \partial_i \partial_j(\rho v_i v_j) = -\partial_i^2 p - \partial_i \partial_j p_{ij}^1. \quad (\text{S3})$$

In the linear response regime, the second term on the left hand side is second order in small quantities and can be dropped. Specializing to one dimension, and taking $\delta n = n - n_0$ with n_0 is the background density, the change in density $\delta n(z, t)$ obeys

$$\partial_t^2 \delta n = \frac{1}{m} \partial_z^2 \delta p + \frac{1}{m} \partial_z^2 p_{zz}^1. \quad (\text{S4})$$

As our initial conditions are isothermal, we find the pressure change $\delta p = p - p_0$ in terms of the changes in the density δn and temperature δT . In this case, the pressure change can be written in the form [23] $\delta p = mc_T^2(\delta n + \delta \tilde{T})$, so that

$$\delta \ddot{n} = c_T^2 \partial_z^2 (\delta n + \delta \tilde{T}) + \frac{1}{m} \partial_z^2 p_{zz}^1. \quad (\text{S5})$$

where $\delta \tilde{T} \equiv n_0 \beta \delta T$ with $\beta = -1/n(\partial n/\partial T)_p$ the expansivity.

Next, we require the evolution equation for δT , which obeys [23],

$$\delta\dot{T} = \epsilon_{LP} \frac{\delta\dot{n}}{\beta n_0} + \frac{\delta\dot{q}}{n_0 c_{V_1}}, \quad (\text{S6})$$

where $\epsilon_{LP} \equiv c_{P_1}/c_{V_1} - 1$ is the Landau-Placzek parameter, which describes the adiabatic change in the temperature arising from the change in density. Here, c_{V_1} , c_{P_1} are the heat capacities per particle. The heat flow per unit volume $\delta\dot{q} = -\partial_z J_E$, where J_E is the energy current, which we determine using a kinetic theory relaxation model in S A 2. Multiplying eq. S6 by $n_0 \beta$, we obtain

$$\delta\dot{T} = \epsilon_{LP} \delta\dot{n} - \frac{\beta}{c_{V_1}} \partial_z J_E. \quad (\text{S7})$$

2. Kinetic theory relaxation model

In this section, we derive the relaxation model equations for a normal phase unitary Fermi gas, which determine how the viscous force and heat current relax to their Navier-Stokes forms. To proceed, we rewrite Eq. S5 as

$$\delta\ddot{n} = c_T^2 \partial_z^2 (\delta n + \delta\tilde{T}) + \delta Q_\eta, \quad (\text{S8})$$

where

$$\delta Q_\eta \equiv \frac{1}{m} \partial_z^2 p_{zz}^1. \quad (\text{S9})$$

Similarly, Eq. S7 is rewritten as

$$\delta\dot{T} = \epsilon_{LP} \delta\dot{n} + \delta Q_\kappa, \quad (\text{S10})$$

with

$$\delta Q_\kappa \equiv -\frac{\beta}{c_{V_1}} \partial_z J_E. \quad (\text{S11})$$

We derive the evolution equations for δQ_η (see Eq. S37) and δQ_κ (see Eq. S53) using a relaxation time approximation for the Boltzmann equation. In this case, the single particle phase space distribution $f(\mathbf{r}, \mathbf{v}, t)$ obeys

$$\partial_t f + \mathbf{v} \cdot \nabla f = -\frac{1}{\tau} (f - f_0) \equiv -\frac{1}{\tau} f_1 \quad (\text{S12})$$

with τ is the relaxation time and $f = f_0 + f_1$, with f_0 the equilibrium distribution.

In the high-temperature Maxwell-Boltzmann limit, the equilibrium distribution is

$$f_0 = n_0 W_0(\mathbf{U}), \quad (\text{S13})$$

where $\mathbf{U} = \mathbf{v} - \mathbf{u}$ is the particle velocity relative to the stream velocity $\mathbf{u}(\mathbf{r}, t)$ and $\int d^3\mathbf{U} W(\mathbf{U}) = 1$. Here,

$$W_0(\mathbf{U}) = \frac{e^{-\mathbf{U}^2/v_0^2}}{(v_0\sqrt{\pi})^3} \quad (\text{S14})$$

and $v_0 = \sqrt{2k_B T/m}$ is the thermal speed. In general, the background temperature T_0 spatially varies $T \equiv T(\mathbf{r})$. For convenience, we drop the subscript 0 and use T for the temperature in deriving the relaxation equations.

Without specifying the phase space distribution f , the pressure tensor is given by

$$p_{ij} = m \int d^3\mathbf{U} U_i U_j f(\mathbf{r}, \mathbf{v}, t). \quad (\text{S15})$$

Taking $p_{ij} = p_{ij}^0 + p_{ij}^1$, the scalar pressure $p_0 \equiv p$, is immediately obtained from $p_{ij}^0 = \delta_{ij} p$ with $f = f_0$ and $i = j = x$,

$$p = m \int d^3\mathbf{U} U_x^2 f_0. \quad (\text{S16})$$

Writing $\int d^3\mathbf{U} U_x^2 f_0 = n_0 \langle U_x^2 \rangle \equiv n_0 \overline{U_x^2}$, we have

$$p = n_0 m \overline{U_x^2}, \quad (\text{S17})$$

which gives $p \rightarrow n_0 k_B T_0$ in the Maxwell-Boltzmann limit, Eq. S14.

a. *Shear viscosity*

We find the relaxation equation for δQ_η of Eq. S9 from that of p_{ij}^1 , assuming that the stream velocity $u(\mathbf{r}, t)$ is position dependent, producing a shear stress. Here, we assume that the background temperature T_0 is spatially constant. To proceed, we first consider Eq. S15 for $i \neq j$. The equilibrium distribution f_0 is a symmetric function of \mathbf{U} , so that

$$\int d^3\mathbf{U} U_i U_j f_0 = 0. \quad (\text{S18})$$

Then Eq. S15 with $f = f_0 + f_1$ and Eq. S18 yield

$$p_{ij}^1 = m \int d^3\mathbf{U} U_i U_j f = m \int d^3\mathbf{U} U_i U_j f_1. \quad (\text{S19})$$

Multiplying Eq. S12 by $\int d^3\mathbf{U} U_i U_j$ and using Eq. S19, we obtain

$$\dot{p}_{ij}^1 + m \int d^3\mathbf{U} U_i U_j v^k \partial_k f = -\frac{1}{\tau_\eta} p_{ij}^1, \quad (\text{S20})$$

where we define $\tau \equiv \tau_\eta$ for the shear viscosity. Then,

$$\dot{p}_{ij}^1 + \frac{1}{\tau_\eta} p_{ij}^1 = -I_{ij}, \quad (\text{S21})$$

where

$$I_{ij} = m \int d^3\mathbf{U} U_i U_j v^k \partial_k f = m \int d^3\mathbf{U} U_i U_j v^k \frac{\partial U^l}{\partial x^k} \frac{\partial f}{\partial U^l}. \quad (\text{S22})$$

For fast relaxation, where $f_1 \rightarrow \tau_\eta v_k \partial_k f$ in Eq. S12, we see that $p_{ij}^1 \simeq \tau_\eta I_{ij}$ is already first order in τ_η , so that we can take $f \rightarrow f_0$ in Eq. S22. Using $\mathbf{U} = \mathbf{v} - \mathbf{u}$,

$$\frac{\partial U^l}{\partial x^k} = -\frac{\partial u^l}{\partial x^k}. \quad (\text{S23})$$

Then with $v_k = U_k + u_k$ in Eq. S22, we obtain

$$I_{ij} = -m \frac{\partial u^l}{\partial x^k} \int d^3\mathbf{U} U_i U_j (U_k + u_k) \frac{\partial f_0}{\partial U^l}. \quad (\text{S24})$$

Integrating by parts, we then have

$$I_{ij} = m \frac{\partial u^l}{\partial x^k} \int d^3\mathbf{U} \frac{\partial}{\partial U^l} [U_i U_j (U_k + u_k)] f_0, \quad (\text{S25})$$

Using $\partial U_i / \partial U_l = \delta_{il}$ and defining $\int d^3\mathbf{U} g(\mathbf{U}) f_0(\mathbf{U}) = n_0 \langle g(\mathbf{U}) \rangle$, Eq. S25 can be rewritten as

$$I_{ij} = m \frac{\partial u^l}{\partial x^k} n_0 \{ \delta_{il} \langle U_j (U_k + u_k) \rangle + \delta_{jl} \langle U_i (U_k + u_k) \rangle + \delta_{kl} \langle U_i U_j \rangle \} \quad (\text{S26})$$

Eq. S26 is simplified with

$$n_0 \langle U_j (U_k + u_k) \rangle = \int d^3\mathbf{U} U_j (U_k + u_k) f_0 = n_0 \delta_{jk} \overline{U_x^2}, \quad (\text{S27})$$

where the u_k term vanishes since f_0 is symmetric in U_j . Hence, we can write $\langle U_i U_j \rangle = \delta_{ij} \overline{U_x^2}$. With $p = n_0 m \overline{U_x^2}$ from Eq. S17, we have

$$I_{ij} = p \frac{\partial u^l}{\partial x^k} \{ \delta_{il} \delta_{jk} + \delta_{jl} \delta_{ik} + \delta_{kl} \delta_{ij} \}. \quad (\text{S28})$$

Carrying out the sums over repeated indices, we obtain

$$I_{ij} = p \left(\frac{\partial u^i}{\partial x^j} + \frac{\partial u^j}{\partial x^i} + \delta_{ij} \nabla \cdot \mathbf{u} \right), \quad (\text{S29})$$

where the δ_{ij} term vanishes for $i \neq j$.

To determine p_{ij}^1 for all i, j , we consider the symmetric second rank traceless pressure tensor,

$$p_{ij}^1 \rightarrow m \int d^3 \mathbf{U} \left(U_i U_j - \frac{1}{3} \delta_{ij} \mathbf{U}^2 \right) f_1. \quad (\text{S30})$$

where the f_0 part of f vanishes because it is scalar function of \mathbf{U} . Since $\mathbf{U}^2 = \text{Tr}\{U_i U_j\}$, evaluating Eq. S30 just changes I_{ij} in Eq. S21 and Eq. S29 to

$$I_{ij} \rightarrow I_{ij} - \frac{1}{3} \delta_{ij} \text{Tr}\{I_{ij}\} \equiv p \sigma_{ij}. \quad (\text{S31})$$

The δ_{ij} term in Eq. S29 makes no contribution to the symmetric traceless tensor, yielding

$$\sigma_{ij} = \frac{\partial u^i}{\partial x^j} + \frac{\partial u^j}{\partial x^i} - \frac{2}{3} \delta_{ij} \nabla \cdot \mathbf{u}. \quad (\text{S32})$$

With Eqs. S31 and S32, Eq. S21 determines the relaxation equation for the shear stress tensor,

$$\dot{p}_{ij}^1 + \frac{1}{\tau_\eta} p_{ij}^1 = -p \sigma_{ij}. \quad (\text{S33})$$

For small τ_η , $\dot{p}_{ij}^1 \ll p_{ij}^1/\tau_\eta$, we see that

$$p_{ij}^1 \rightarrow -\tau_\eta p \delta_{ij} = -\eta \sigma_{ij}, \quad (\text{S34})$$

where the static shear viscosity is

$$\eta = \tau_\eta p. \quad (\text{S35})$$

Now we can evaluate the relaxation equation for δQ_η of Eq. S9. We evaluate Eq. S32 for σ_{zz} and eliminate the velocity field using current conservation Eq. S1. To first order in small quantities, $\delta \dot{n} + n_0 \partial_z v_z = 0$, yielding

$$\sigma_{zz} = \frac{4}{3} \partial_z v_z = -\frac{4}{3} \frac{\delta \dot{n}}{n_0}. \quad (\text{S36})$$

We find $\delta \dot{Q}_\eta$ using Eq. S9, $\delta Q_\eta \equiv \frac{1}{m} \partial_z^2 p_{zz}^1$. With Eq. S36 and Eq. S33 we obtain finally,

$$\delta \dot{Q}_\eta + \frac{1}{\tau_\eta} \delta Q_\eta = \frac{4}{3} \frac{p}{m n_0} \partial_z^2 \delta \dot{n}. \quad (\text{S37})$$

For fast relaxation, $\delta \dot{Q}_\eta \ll \delta Q_\eta/\tau_\eta$, we find,

$$\delta Q_\eta \rightarrow \frac{4}{3} \frac{\tau_\eta p}{m n_0} \partial_z^2 \delta \dot{n} = \frac{4}{3} \frac{\eta}{m n_0} \partial_z^2 \delta \dot{n}. \quad (\text{S38})$$

In this limit, Eq. S8 with Eq. S38 reproduces the Navier-Stokes form used in Ref. [23]. We note that Eq. S35 for η and Eq. S37 for $\delta \dot{Q}_\eta$ are *independent* of the form of the single particle phase space distribution, $f_0(\mathbf{r}, \mathbf{v})$, which has not been explicitly used to obtain the background pressure p from Eq. S17.

b. Thermal conductivity

Next, we find the relaxation equation for δQ_κ of Eq. S11 from that of the 1D energy current, J_E ,

$$J_E = \int d^3 \mathbf{v} v_z \frac{m}{2} \mathbf{v}^2 f. \quad (\text{S39})$$

To find the relaxation equation of the energy current, we assume that the system is in mechanical equilibrium with a stream velocity $\mathbf{u} = 0$, so that $\mathbf{U} = \mathbf{v}$ in Eq. S14, and we include a temperature gradient $T(\mathbf{r})$. Eq. S39 shows that J_E vanishes for $f = f_0$, since the integrand would be odd in v_z .

Using Eq. S39 and Eq. S12 with $\tau \equiv \tau_\kappa$, we have

$$\dot{J}_E + \frac{m}{2} \partial_z \int d^3\mathbf{v} v_z^2 \mathbf{v}^2 f_0 = -\frac{1}{\tau_\kappa} J_E \quad (\text{S40})$$

or

$$\dot{J}_E + \frac{1}{\tau_\kappa} J_E = -\partial_z I_{zz}. \quad (\text{S41})$$

Here

$$I_{zz} \equiv \frac{m}{2} \int d^3\mathbf{v} v_z^2 \mathbf{v}^2 f_0. \quad (\text{S42})$$

To evaluate Eq. S42, we require an explicit form for the equilibrium phase space distribution, which we take to be a Maxwell-Boltzmann distribution, $f_0(\mathbf{r}, \mathbf{v}) = n(\mathbf{r}) W_0(\mathbf{v})$, where

$$W_0(\mathbf{v}) = \frac{e^{-\mathbf{v}^2/v_0^2}}{(v_0\sqrt{\pi})^3} \quad (\text{S43})$$

with $v_0 = \sqrt{2k_B T/m}$ the thermal speed. As discussed above, we assume that $T = T(\mathbf{r})$ spatially varies, producing a temperature gradient, as discussed further below. Then,

$$I_{zz} = \frac{m}{2} \frac{1}{3} \langle v^4 \rangle n(\mathbf{r}). \quad (\text{S44})$$

Here,

$$\langle v^4 \rangle = \int d^3\mathbf{v} v^4 W_0(\mathbf{v}) = \frac{4}{\sqrt{\pi}} v_0^4 \int d\left(\frac{v}{v_0}\right) \left(\frac{v}{v_0}\right)^6 e^{-(v/v_0)^2}, \quad (\text{S45})$$

which yields

$$\langle v^4 \rangle = \frac{15}{4} v_0^4 = 15 \left(\frac{k_B T}{m}\right)^2. \quad (\text{S46})$$

Using Eq. S46 in Eq. S44, and the pressure $p(\mathbf{r}) = n(\mathbf{r}) k_B T(\mathbf{r})$ from Eqs. S17 and S43, we have

$$I_{zz} = \frac{5}{2} \frac{k_B}{m} n(\mathbf{r}) k_B T^2(\mathbf{r}) = \frac{5}{2} \frac{k_B}{m} p(\mathbf{r}) T(\mathbf{r}). \quad (\text{S47})$$

With Eq. S41, we then obtain

$$\dot{J}_E + \frac{1}{\tau_\kappa} J_E = -\frac{5}{2} \frac{k_B}{m} \partial_z [p(\mathbf{r}) T(\mathbf{r})]. \quad (\text{S48})$$

For pure heat flow, mechanical equilibrium requires

$$\nabla p(\mathbf{r}) = 0. \quad (\text{S49})$$

Therefore, Eq. S48 becomes

$$\dot{J}_E + \frac{1}{\tau_\kappa} J_E = -\frac{5}{2} \frac{k_B}{m} p \partial_z \delta T, \quad (\text{S50})$$

where we suppress the argument \mathbf{r} . Here, the temperature $T = T_0 + \delta T$, with T_0 the uniform background temperature, so that $\partial_z T = \partial_z \delta T$.

For fast relaxation, where $\dot{J}_E \ll J_E/\tau_\kappa$, Eq. S50 gives

$$J_E \rightarrow -\frac{5}{2} \frac{k_B}{m} \tau_\kappa p \partial_z \delta T \equiv -\kappa_T \partial_z \delta T, \quad (\text{S51})$$

where the static thermal conductivity is

$$\kappa_T = \frac{5}{2} \frac{k_B}{m} \tau_\kappa p. \quad (\text{S52})$$

We find $\delta\dot{Q}_\kappa$ using Eq. S11, $\delta Q_\kappa \equiv -(\beta/c_{V_1}) \partial_z J_E$. Then, operating on Eq. S50 with $-(\beta/c_{V_1}) \partial_z$, we have

$$\delta\dot{Q}_\kappa + \frac{1}{\tau_\kappa} \delta Q_\kappa = \frac{5}{2} \frac{k_B}{m} \frac{p}{n_0 c_{V_1}} \partial_z^2 \delta\tilde{T}, \quad (\text{S53})$$

where $\delta\tilde{T} = n_0 \beta \delta T$ (see Eq. S5). For fast relaxation, where $\delta\dot{Q}_\kappa \ll \frac{1}{\tau_\kappa} \delta Q_\kappa$, Eq. S53 gives

$$\delta Q_\kappa \rightarrow \frac{5}{2} \frac{k_B}{m} \frac{\tau_\kappa p}{n_0 c_{V_1}} \partial_z^2 \delta\tilde{T} = \frac{\kappa_T}{n_0 c_{V_1}} \partial_z^2 \delta\tilde{T}. \quad (\text{S54})$$

In this limit, Eq. S10 with Eq. S54 reproduces the Navier-Stokes form used in Ref. [23]. We note that the coefficient 5/2 in Eq. S52 for κ_T and in Eq. S53 for $\delta\dot{Q}_\kappa$ is dependent on the assumed Maxwell-Boltzmann approximation for the phase space distribution f_0 , which was needed to evaluate Eq. S42, yielding Eq. S47.

3. Relaxation of the Fourier Components

In the experiments, as described in the main text, a spatially periodic perturbing potential δU is used to create a spatially periodic density perturbation $\delta n(z, t = 0)$, with a wavelength λ and corresponding wavevector $q = 2\pi/\lambda$. After the system reaches mechanical and thermal equilibrium, δU is abruptly extinguished and $\delta n(z, t)$ is measured. A spatial Fourier transform of the relaxing density perturbation $\delta n(z, t)$ yields the time dependence of the Fourier component, $\delta n(q, t)$. The evolution of $\delta n(q, t)$ is readily determined from the Fourier transforms of Eqs. S8, S37, S10 and S53. Defining $\delta n(q, t) \equiv \delta n$, $\delta\tilde{T}(q, t) \equiv \delta\tilde{T}$, $\delta Q_\eta(q, t) \equiv \delta Q_\eta$, and $\delta Q_\kappa(q, t) \equiv \delta Q_\kappa$, we find

$$\delta\ddot{n} = -\omega_T^2 \delta n - \omega_T^2 \delta\tilde{T} + \delta Q_\eta \quad \text{with} \quad \omega_T \equiv c_T q, \quad (\text{S55})$$

$$\delta\dot{Q}_\eta = -\frac{1}{\tau_\eta} \delta Q_\eta - \Omega_\eta^2 \delta\dot{n} \quad \text{with} \quad \Omega_\eta^2 \equiv \frac{4}{3} \frac{p}{m n_0} q^2, \quad (\text{S56})$$

and

$$\delta\dot{\tilde{T}} = \epsilon_{LP} \delta\dot{n} + \delta Q_\kappa, \quad \text{where} \quad (\text{S57})$$

$$\delta\dot{Q}_\kappa = -\frac{1}{\tau_\kappa} \delta Q_\kappa - \Omega_\kappa^2 \delta\tilde{T} \quad \text{with} \quad \Omega_\kappa^2 = \frac{5}{2} \frac{k_B}{m} \frac{p}{n_0 c_{V_1}} q^2. \quad (\text{S58})$$

For a unitary Fermi gas, the pressure p and internal energy density \mathcal{E} have the universal forms

$$p = \frac{2}{5} n \epsilon_F(n) f_E(\theta) = \frac{2}{3} \mathcal{E}, \quad (\text{S59})$$

where the universal function $f_E(\theta)$ has been measured [30] as a function of the reduced temperature $\theta \equiv T/T_F$. Here, the local Fermi energy $\epsilon_F(n) = \frac{\hbar^2}{2m} (3\pi^2 n)^{2/3}$ with n the total density for a 50-50 mixture of two spin states. Taking $\epsilon_F(n) = m v_F^2/2$, which defines the Fermi speed v_F , we can write in Eq. S56

$$\Omega_\eta^2 \equiv \frac{4}{15} \omega_F^2 f_E(\theta), \quad (\text{S60})$$

where we define $\omega_F \equiv v_F q$. Similarly, we can write in Eq. S58

$$\Omega_\kappa^2 \equiv \frac{1}{2} \frac{k_B}{c_{V_1}} \omega_F^2 f_E(\theta). \quad (\text{S61})$$

In the short relaxation time limit, we see that $\delta Q_\eta \rightarrow -\gamma_\eta \delta\dot{n}$, with $\gamma_\eta \equiv \tau_\eta \Omega_\eta^2 = \frac{4}{3} \frac{\eta}{n_0 m} q^2$ and $\delta Q_\kappa \rightarrow -\gamma_\kappa \delta\dot{\tilde{T}}$, with $\gamma_\kappa \equiv \tau_\kappa \Omega_\kappa^2 = \frac{\kappa_T}{n_0 c_{V_1}} q^2$, reproducing the results in the supplement of Ref. [23].

The linear time-dependent equations S55, S56, S57, and S58 are easily solved to determine $\delta n(q, t)$, with the initial conditions $\delta n(q, 0) = A$, $\delta T(q, 0) = 0$, $\delta Q_\eta(q, 0) = 0$, and $\delta Q_\kappa(q, 0) = 0$. The data are fit using the amplitude A , isothermal frequency ω_T , and relaxation times τ_η and τ_κ as free parameters. As in our previous experiments [23], the ratio ω_T/ω_F self-consistently determines the reduced temperature θ in the fits.

In the main text, the relaxation times are given in units of the ‘‘Fermi time,’’ which we take to be $\tau_F \equiv \lambda_F/v_F$, i.e., the time for an atom to move a Fermi wavelength at the Fermi speed. With $\lambda_F = 2\pi\hbar/(mv_F)$, and $mv_F^2 = 2\epsilon_F$, the Fermi time is

$$\tau_F = \frac{\pi\hbar}{\epsilon_F}. \quad (\text{S62})$$

4. Static Transport Properties

With the relaxation times determined from the fits, the *static* shear viscosity Eq. S35 is determined in units of $\hbar n_0$ by

$$\eta = \tau_\eta p = \alpha_\eta \hbar n_0, \quad (\text{S63})$$

where Eq. S59 for p gives the dimensionless shear viscosity coefficient,

$$\alpha_\eta = \frac{2\pi}{5} \frac{\tau_\eta}{\tau_F} f_E(\theta). \quad (\text{S64})$$

Similarly, the *static* thermal conductivity Eq. S52 is determined in units of $\hbar n_0 k_B/m$ by

$$\kappa_T = \frac{5}{2} \frac{k_B}{m} \tau_\kappa p = \alpha_\kappa \frac{k_B}{m} \hbar n_0, \quad (\text{S65})$$

where the dimensionless thermal conductivity coefficient is

$$\alpha_\kappa = \pi \frac{\tau_\kappa}{\tau_F} f_E(\theta). \quad (\text{S66})$$

Finally, the first sound diffusivity [23, 33] is determined from the static transport properties,

$$D_1 = \frac{4}{3} \frac{\eta}{n_0 m} + \left(\frac{1}{c_{V_1}} - \frac{1}{c_{P_1}} \right) \frac{\kappa_T}{n_0}. \quad (\text{S67})$$

For a unitary Fermi gas in a 50-50 mixture of two spin states and total density n [22, 23],

$$\frac{1}{c_{V_1}} - \frac{1}{c_{P_1}} = \frac{4}{15} \frac{nT}{p} = \frac{1}{k_B} \frac{2}{3} \frac{\theta}{f_E(\theta)}. \quad (\text{S68})$$

Then

$$\frac{D_1}{\hbar/m} = \frac{4}{3} \alpha_\eta + \frac{2}{3} \frac{\theta}{f_E(\theta)} \alpha_\kappa. \quad (\text{S69})$$

Using Eqs. S64 and S66, we then obtain D_1 in units of \hbar/m from the measured relaxation times,

$$\frac{D_1}{\hbar/m} = \frac{8\pi}{15} \frac{\tau_\eta}{\tau_F} f_E(\theta) + \frac{2\pi}{3} \frac{\tau_\kappa}{\tau_F} \theta. \quad (\text{S70})$$

For comparison with the static transport properties shown in the main text, which are obtained from the measured relaxation times using Eqs. S64, S66, and S70, we parameterize α_η as

$$\alpha_\eta = \alpha_{3/2} \theta^{3/2} + \alpha_{2\eta}. \quad (\text{S71})$$

Here, the first term is the high temperature limit, which is obtained from a variational calculation [4], $\alpha_{3/2} = 45\pi^{3/2}/(64\sqrt{2}) = 2.76849 \simeq 2.77$ and $\alpha_{2\eta}$ is the universal density shift coefficient, which is used as a fit parameter. Similarly, we parameterize α_κ as

$$\alpha_\kappa = \frac{15}{4} \left(\alpha_{3/2} \theta^{3/2} + \alpha_{2\kappa} \right). \quad (\text{S72})$$

Here, the leading factor of $15/4$ is chosen to yield the correct high temperature limit for the ratio κ_T/η . In this limit, Eqs. S65 and S63 yield $\kappa_T = \frac{15}{4} \frac{k_B}{m} \eta$, where we have used $\tau_\kappa/\tau_\eta = 3/2$, which can be shown to hold for any isotropic collision cross section.

With Eqs. S71 and S72, the relaxation times are then parameterized in the main text by inverting Eqs. S64 and S66 as

$$\frac{\tau_\eta}{\tau_F} = \alpha_\eta \frac{5}{2\pi} \frac{1}{f_E(\theta)} \quad (\text{S73})$$

and

$$\frac{\tau_\kappa}{\tau_F} = \alpha_\kappa \frac{1}{\pi} \frac{1}{f_E(\theta)}. \quad (\text{S74})$$

Fig. S1 shows the sound diffusivity obtained from the measured relaxation times, Eq. S70, which is compared to the sound diffusivity measured for sound attenuation by Patel et al., in Ref. [22]. We see that the high temperature behavior obtained from Eq. S69 using the fitted density shift coefficients for the shear viscosity and thermal conductivity in Eqs. S71 and S72 is in good agreement with the high temperature sound attenuation measurements. However, the lower temperature sound diffusivity measurements of Ref. [22] exhibit a nearly constant upward shift relative to the sound diffusivity obtained from the relaxation time experiments.

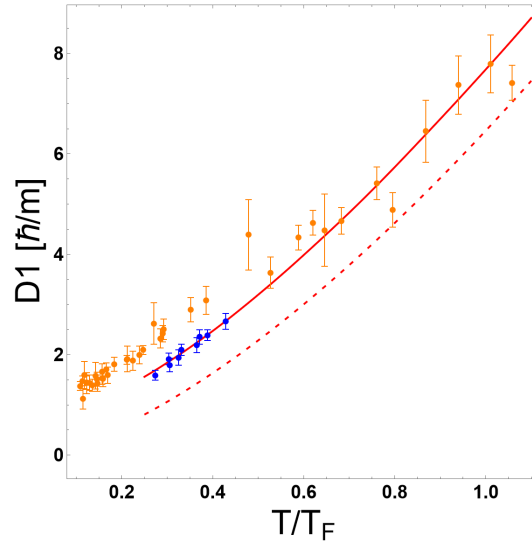


FIG. S1. Sound diffusivity from measured τ_η , τ_κ , $D_1[\hbar/m] = \frac{8\pi}{15} \frac{\tau_\eta}{\tau_F} f_E(\theta) + \frac{2\pi}{3} \frac{\tau_\kappa}{\tau_F} \theta$ (Blue dots), in units of \hbar/m versus reduced temperature $\theta = T/T_F$. Red solid curve: $D_1[\hbar/m] = \frac{4}{3} (2.77 \theta^{3/2} + 0.44) + \frac{5}{2} \frac{\theta}{f_E(\theta)} (2.77 \theta^{3/2} + 0.22)$. Red-dashed curve (high temperature limit): $f_E(\theta) \rightarrow \frac{5}{2} \theta$, $D_1[\hbar/m] = 7/3 \times 2.77 \theta^{3/2}$. Sound diffusivity data of Ref. [22] (Orange dots). Error bars (blue dots) are statistical. (color online)